CHAPTER III
RESULTS AND DISCUSSION

3.1 Preparation Methods

Tensile and impact testing of PP3/2/y/10 composites were carried out in order to evaluate two sets of composites prepared by the old method and the new method.

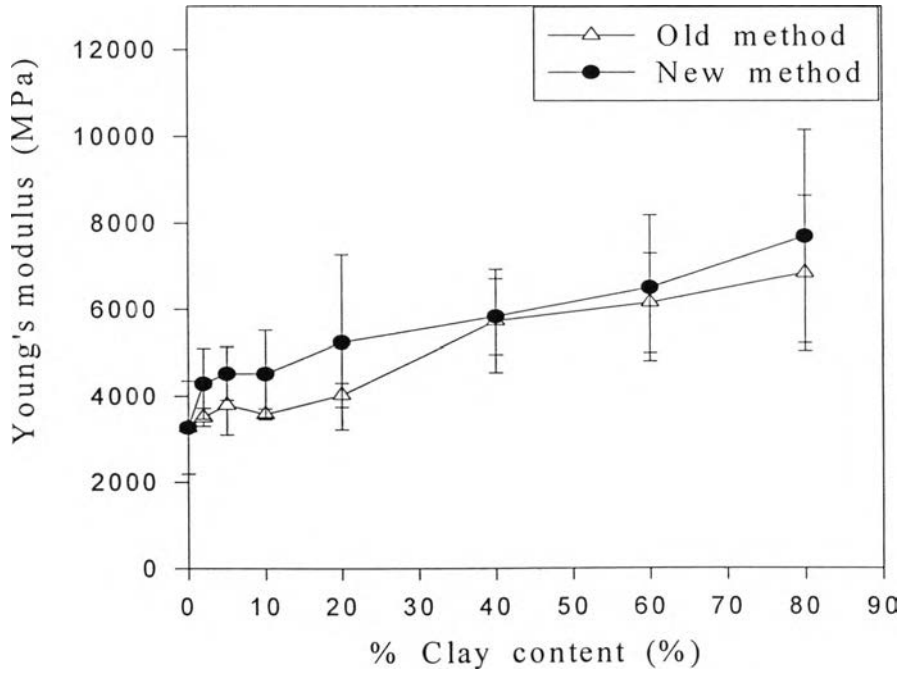

Figure 3.1 Young's modulus of PP3/2/y/10 composites at 26°C prepared from the old method and the new method.

Figure 3.1 shows the Young's modulus of PP nanocomposites as a function of clay content at fixed 10 wt % filler; two preparation methods were carried out. In both methods, the Young's modulus increases with wt % clay content. This is due to the higher stiffness of clay in the filler which is dispersed in the composite. There is no significant difference in Young's modulus at any clay content of the nanocomposites prepared from the two methods.

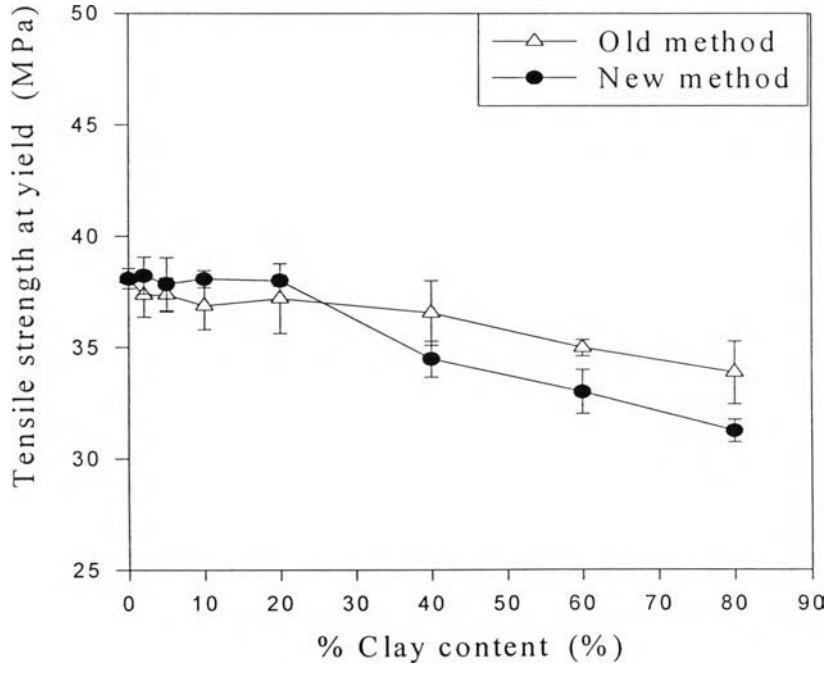

Figure 3.2 Tensile strength at yield of PP3/2/y/10 composites at 26°C prepared from the old method and the new method.

Figure 3.2 shows the tensile strength at yield of PP3/2/y/10 composites as a function of clay content. There is a decrease in tensile strength at yield with clay content for the composites prepared by both methods. This is because there are a lesser number molecular bridgings between crystals. The ability to transfer stress of the PP can be expected to decrease.

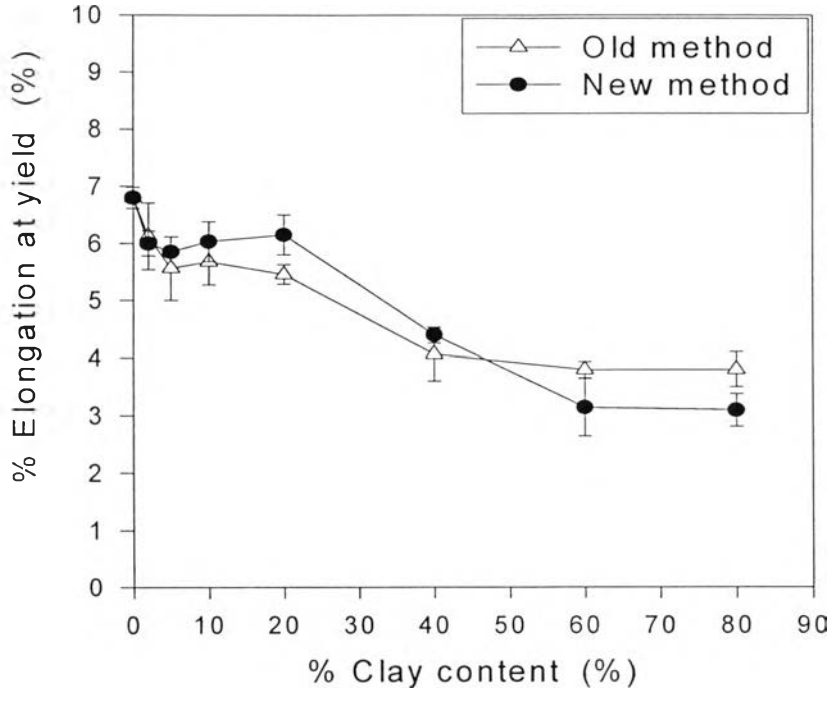

Figure 3.3 The percentage of elongation at yield of PP3/2/y/10 composites at 26°C prepared from the old method and the new method.

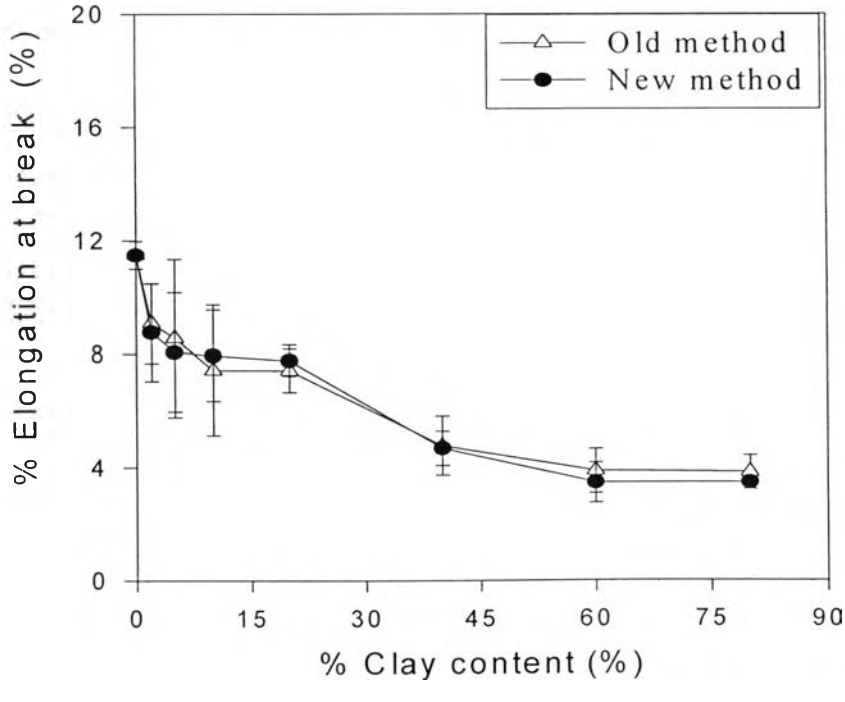

Figure 3.4 The percentage of elongation at break of PP3/2/y/10 composites at 26°C prepared from the old method and the new method.

Figures 3.3 and 3.4 show the % elongation at yield and % elongation at break of PP3/2/y/10 composites prepared from the old and the new methods. The results indicate the same trend; % elongation decreases with wt % clay content. The decrease in wt % elongation arises from the fact that the actual elongation experienced by the polymer matrix is much greater than the measured elongation of the composites. The filler is elongated at a smaller extent than the PP matrix. With more % clay content, the fillers have lesser molecular bridgings, and the ability to transfer stress decreases. Both preparation methods provide composites with nearly the same % elongation at yield and % elongation at break at all % clay contents.

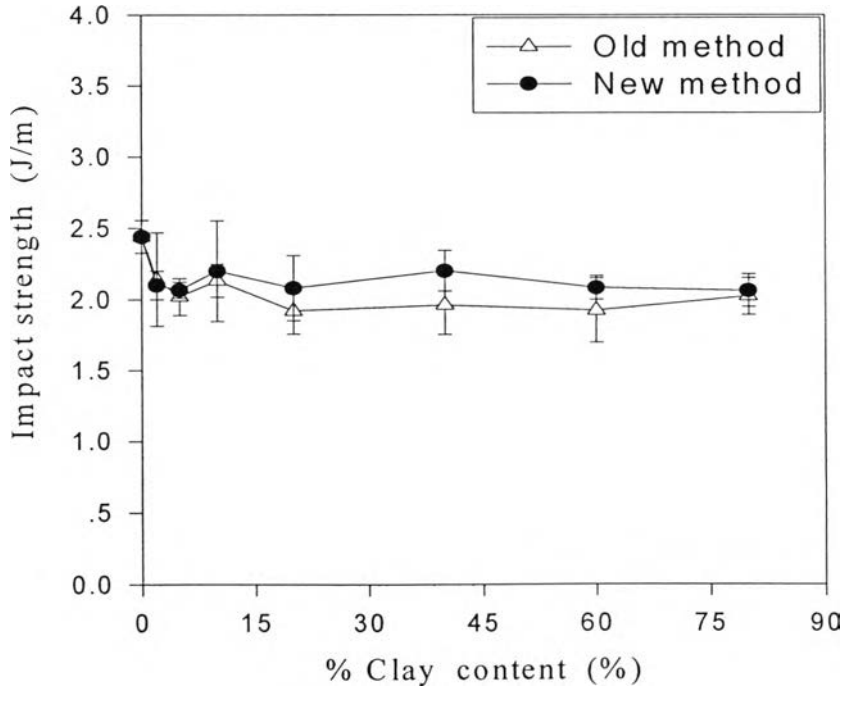

Figure 3.5 Impact strength of PP3/2/y/10 composites at 26°C prepared from the old method and the new method.

The impact strength of PP3/2/y/10 composites prepared from the old method and the new method is shown in Figure 3.5. The impact strength of the composite at first decreases slightly as a small amount of clay is added and then

it becomes independent of wt % clay content. The reduction in impact strength with volume fraction of clay content added is possibly caused by: a) the increase in stress concentrations around the clay particles; b) the increase in the free volume of the composites. The impact strengths of the composites prepared from the old and the new method are nearly the same.

From Figures 3.1-3.5, it can be concluded that the tensile and impact properties of PP3/2/y/10 composites prepared from the old method and new method are nearly the same. In a subsequent study, I used the old method to prepare the composite.

3.2 Characterization Results

3.2.1 The Characterization of Modified Silicate Clay

Powder samples of silicate clay and modified silicate clay were characterized by X-ray diffraction for the determination of the grafting reaction between aminosilane coupling agent and silicate clay.

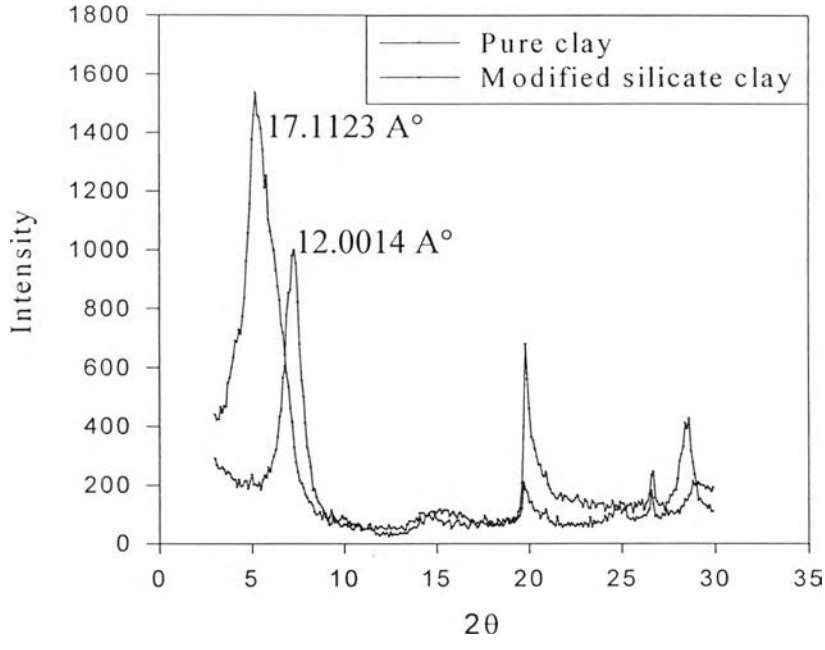

Figure 3.6 XRD intensity versus angle for pure clay and the modified silicate clay.

Figure 3.6 shows the X-ray diffraction patterns of the silicate clay and the modified silicate clay indicating the grafting of aminosilane onto the silicate clay. From this figure, the basal spacing of the modified silicate clay is about 17.1123 A°, longer than that of the pure silicate clay which is 12.0014 A° The expansion of interlayer spacing between crystal indicates that aminosilane coupling agent intercalates into the silicate layers. The expansion in the interlayer spacing can be depicted as shown in Figure 3.7.

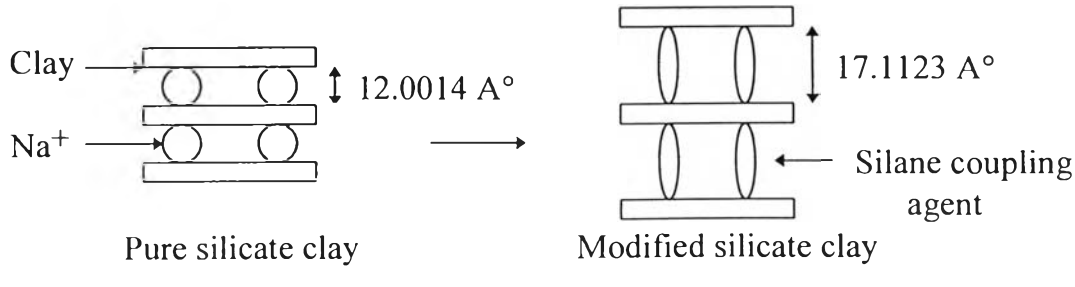

Figure 3.7 Intercalating behavior of clay (Na^+ montmorillonite).

3.2.2 The Characterization of the Grafting MAPP to the Modified Silicate Clay

3.3.2.1 X-Ray Diffraction Results. The delamination of the silicate clay in the nanofiller was confirmed by X-ray diffraction (XRD) results. Figure 3.8 shows the XRD pattern of the mixture of modified silicate clay with MAPP (the maleic anhydride modified polypropylene). The plane peaks shifts to lower angles or higher basal spacing. The basal spacing of the filler are 22.9614 A° and 15.1862 A°. This result suggests that the interlayer spacing is possibly expanded by the interpenetration of the polymer into the basal spacing of the modified silicate clay as in Figure 3.9.

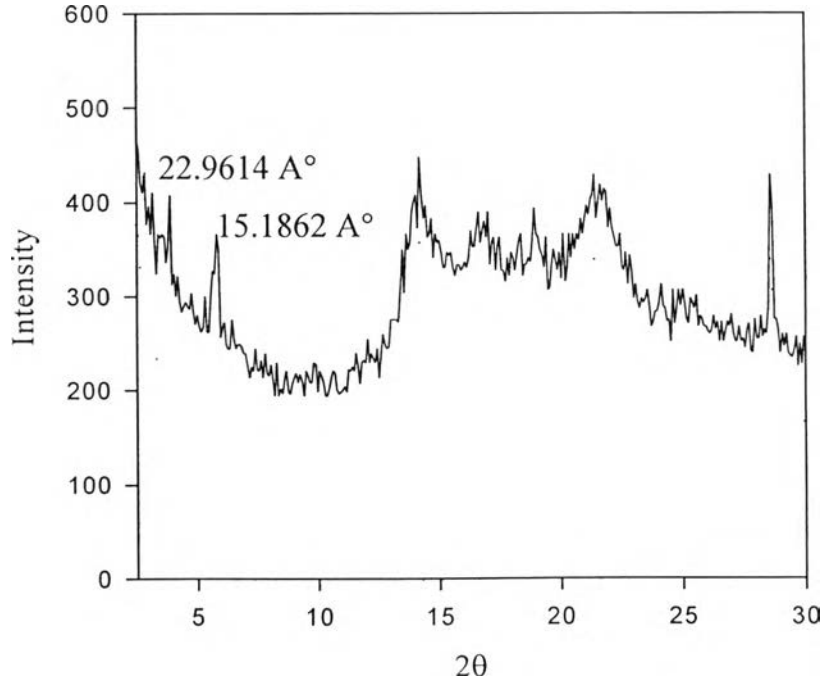

Figure 3.8 XRD intensity versus angle for the filler prepared from modified clay and MAPP.

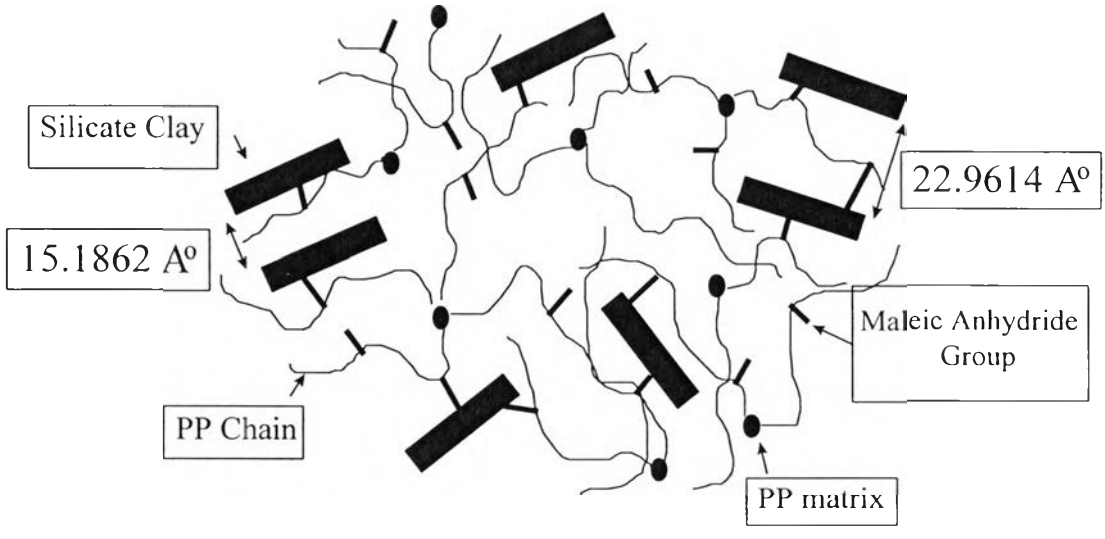

Figure 3.9 Model of the MAPP chain grafted filler.

3.2.2.2 DRIFT Results. The possibility of the reaction between the silane coupling agent attached onto silicate clay and the MAPP were carried out. Diffuse reflectance infrared spectroscopy (DRIFT) was used to characterize this reaction.

The IR spectra in Figure 3.10 shows the results of pure MAPP, a filler containing 5 wt % clay content and a filler containing 20 wt % clay content. The MAPP is depicted as the lowest line. The carbonyl peak of anhydride group appears in two peaks. One peak is 1717.73 cm^{-1}, and another peak is 1779.7 cm^{-1}. The two upper infrared absorbance spectra shown in Figure 3.10 are assigned to the MAPP grafted with the modified silicate clay. In these two spectra, the two peaks of anhydride disappear but a new peak appears at about 1600 cm^{-1}. This peak corresponds to carbonyl peak of amide group of the filler.

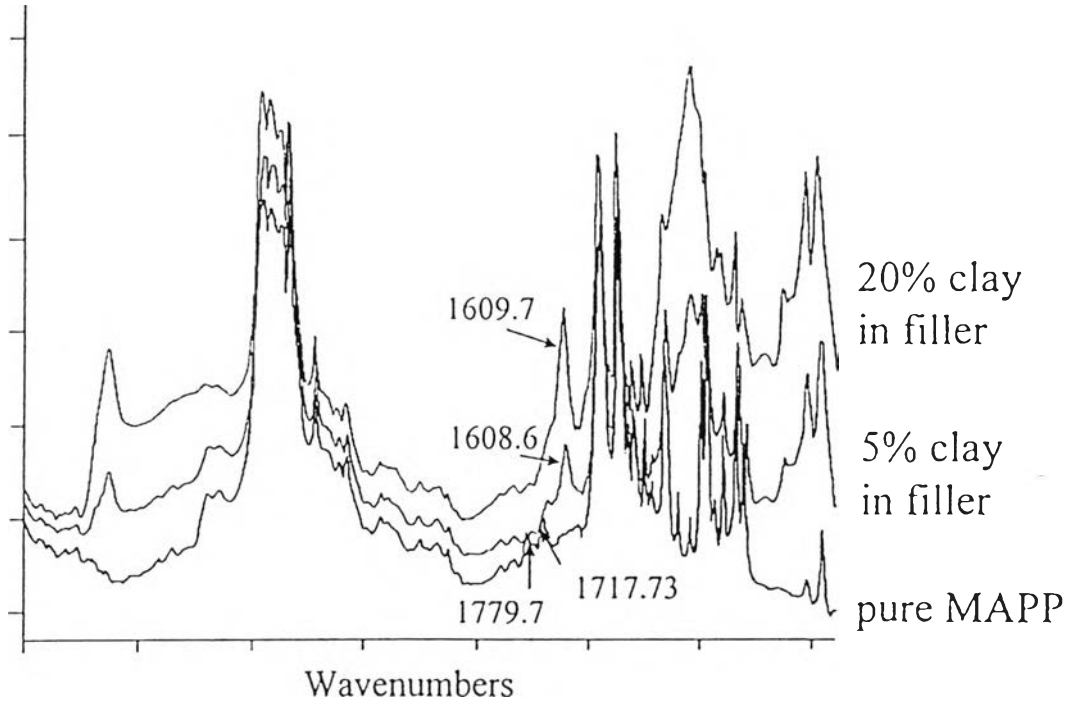

Figure 3.10 DRIFT results of MAPP, filler containing 5 percent by weight clay and filler containing 20 percent by weight clay.

From the above results, we confirm the grafting reaction according to this equation:

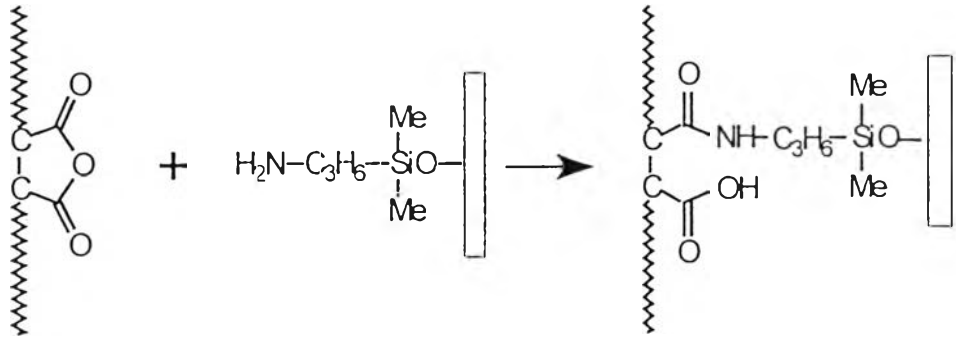

MAPP Modified silicate clay Nanofiller

3.2.2.3 TEM Result. The TEM micrograph of a section of PP1/2/10/2 composites is shown in Figure 3.11. This photograph shows that the silicate paritcles are finely dispersed, some individually and some are stacked in thin layers. From the photograph the intersection of individual layers is about 20 nm and the intersection of thickest dark layer is about 60 nm. The irregular shape of the particles indicates stacking and aggregation of individual layers.

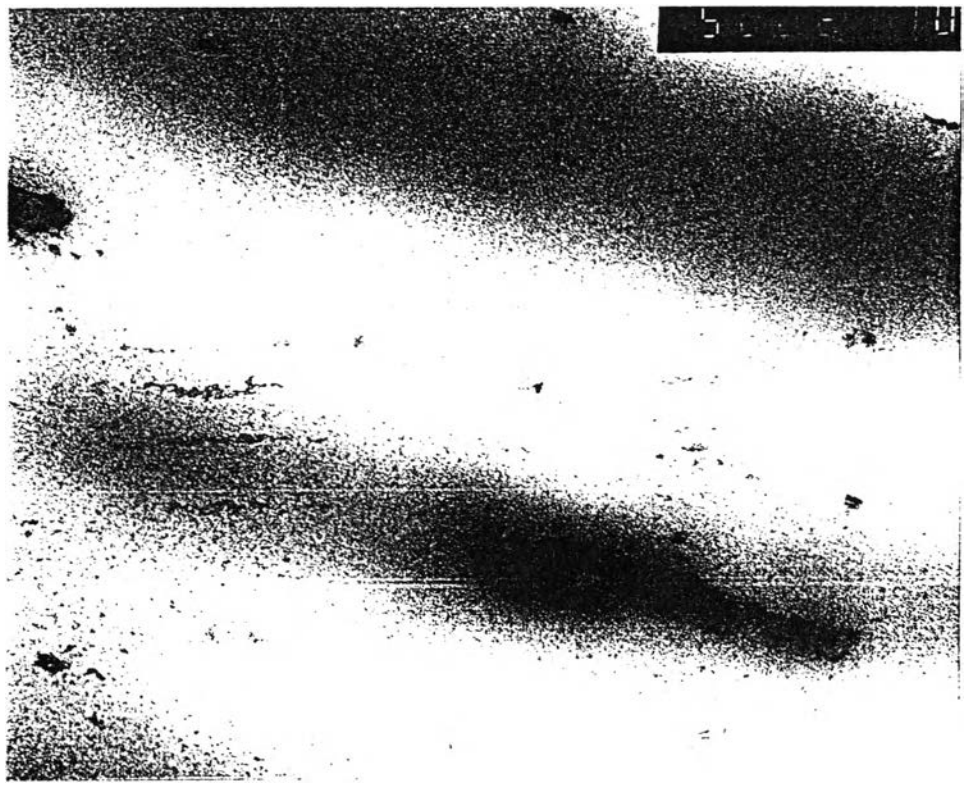

Figure 3.11 TEM micrograph of PP1/2/10/2 composites.

3.3 Mechanical Properties Results

Tensile, Impact and slow crack growth properties were measured to determine optimum preparation conditions and the appropiate amount of clay and filler in the nanocomposites.

3.3.1 Tensile and Impact Properties

3.3.1.1 The Effect of Filler Content and Clay Content. Three sets of the PP1 composite were tested as a function of filler content at fixed 10, 60 and 100 wt % clay contents.

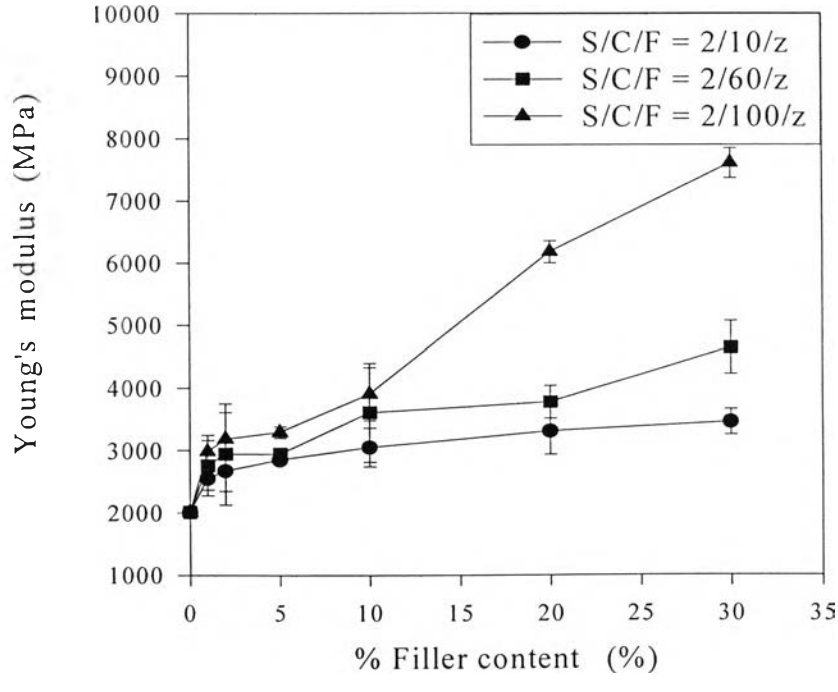

Figure 3.12 Effect of filler content on Young's modulus of PP1 composites at 26°C.

Figure 3.12 shows the Young's modulus of PP1 composites as a function of filler content at fixed 10, 60 and 100 wt % clay contents. The Young's modulus increases with both filler content and clay content. This is

due to the higher stiffness of clay which induces the composite to be more stiffer and therefore having higher Young's modulus values.

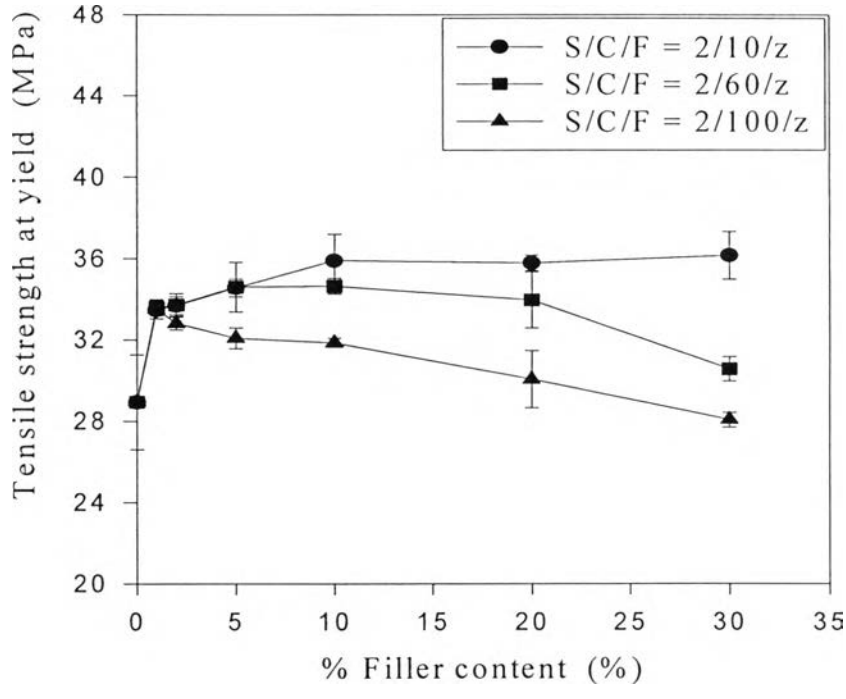

Figure 3.13 Effect of filler content on tensile strength at yield of PP1 composites at 26°C.

Figure 3.13 shows the tensile strength at yield of PP1composite as a function of filler content at fixed 10, 60 and 100 % clay contents. The results show that at low percentage of filler content, the tensile strength at yield increases and then decreases with increasing filler content. This trend is opposite to that of the Young's modulus in Figure 3.12. This is due to reduction in volume fraction of PP matrix with increasing filler content. At a fixed amount of the filler content, the tensile strength at yield of the composite decreases with clay content. This is because a lesser number of molecular bridging occurs between PP crystalline domains as the amount of MAPP becomes less. For these composites, they become less ductile with increasing filler content.

The percentage of elongation at yield of PP1 composites as a function of filler content at fixed 10, 60 and 100 wt % clay contents was plotted in Figure 3.14. The percentage of elongation at yield , monotonically decreases with filler content and clay content. Since the elongation of filler is less than that of PP matrix, we can expect less ductile behavior with more clay and filler contents.

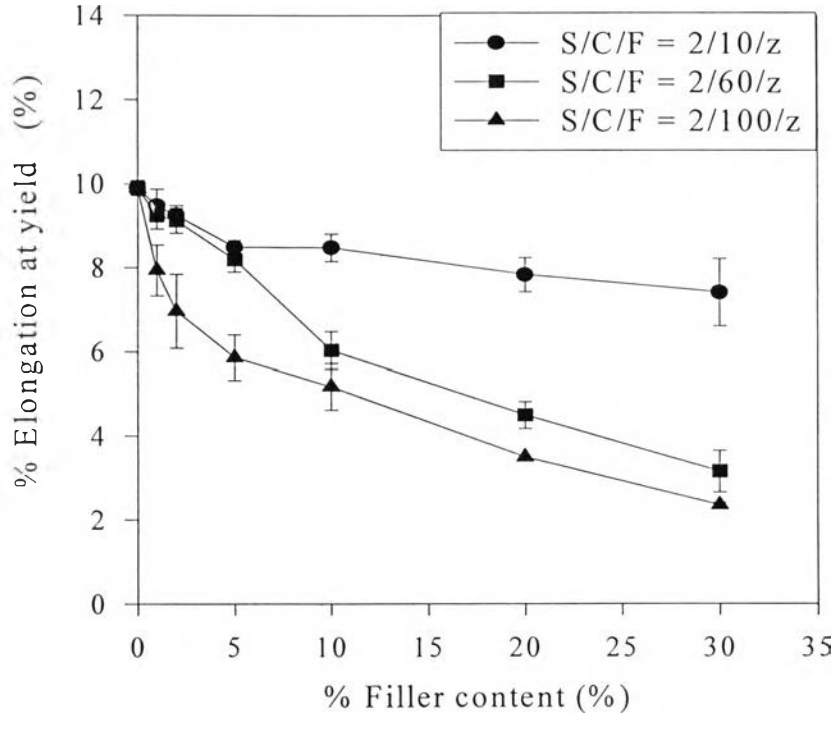

Figure 3.14 Effect of filler content on % elongation at yield of PP1 composites at 26°C.

Figure 3.15 shows the percentage of elongation at break of PP1 composite as a function of filler content at fixed 10, 60 and 100 wt % clay contents. The plot shows that the percentage of elongation at break increases at low wt % filler content up to an optimal point as shown in Table 1, then the percentage of elongation at break decreases with filler content. At any filler contents, the percentage of elongation at break decreases with clay content. This is because at low percentage of filler and clay contents, there is a good

adhesion between filler and PP matrix and the good effect of tie molecules, the percentage of elongation at break is greater. After the optimum point, the inclusion of the filler results in decreasing percent elongation at break.

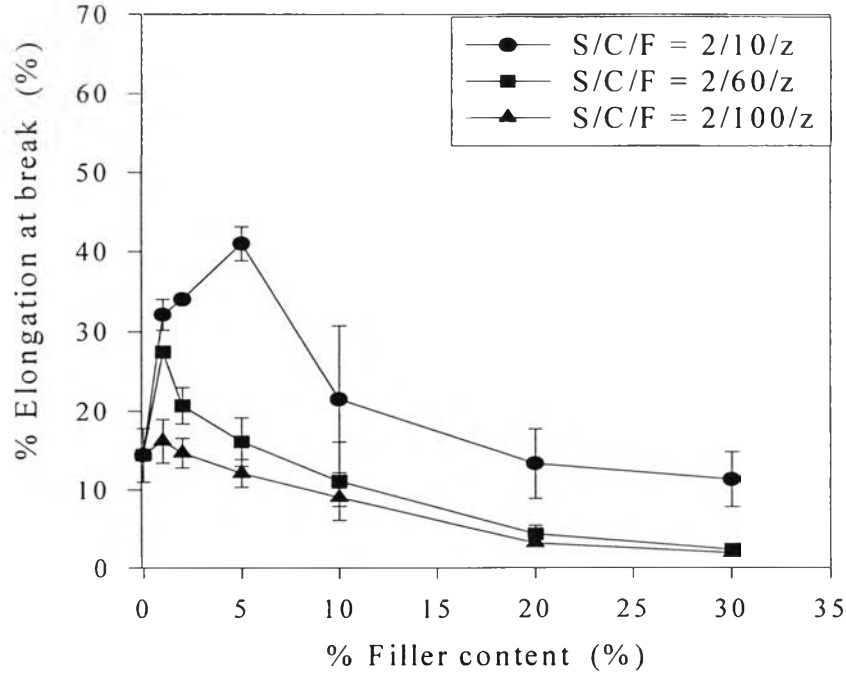

Figure 3.15 Effect of filler content on percent elongation at break of PP1 composites at 26°C.

Table 3.1 Optimal conditions of percent elongation at break of each composite

Composites	Optimal condition
PP1/2/10/z	5 % filler content
PP1/2/60/z	1 % filler content
PP1/2/100/z	1% filller content

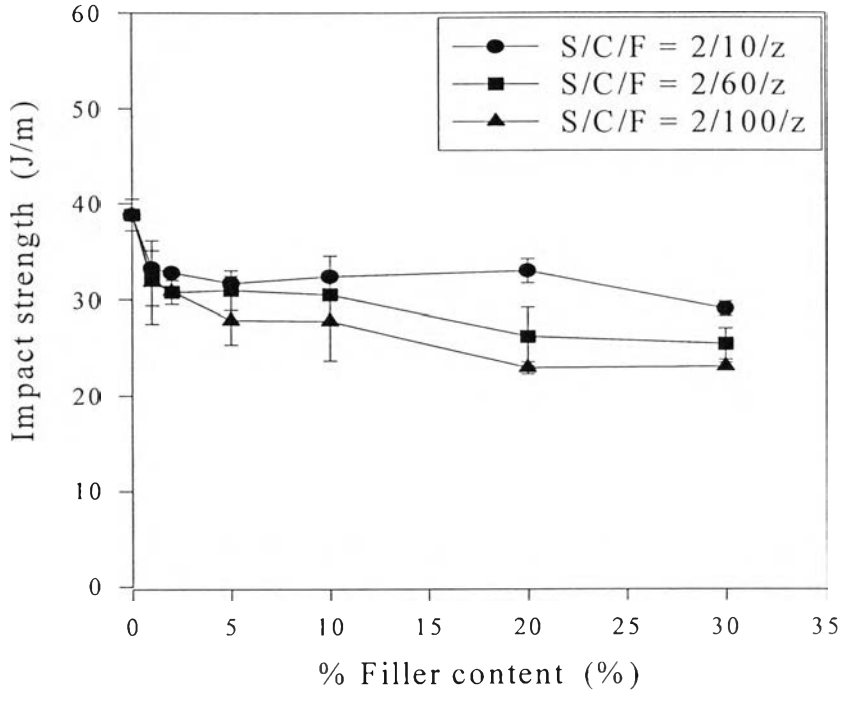

Figure 3.16 Effect of filler content on impact strength of PP1/2/10/z, PP1/2/60/z and PP1/2/100/z composites at 26°C.

Figure 3.16 shows the impact strength of PP1 composite as a function of filler content at fixed 10, 60, 100 wt % clay contents. From this figure, the impact strength of composite is lower than pure PP; it decreases with clay content. It is clear that the filler makes the composite more brittle and absorbs less energy because the filler acts as a stress concentrator.

3.3.1.2 The Effect of M_W of PP Matrix. The PP1 and PP3 composites were tested as a function of clay content at fixed 10 wt % filler content to study the effect of M_W of PP matrix. The M_W of PP1 is about 840,000 that is greater than the M_W of PP3 which is about 420,000.

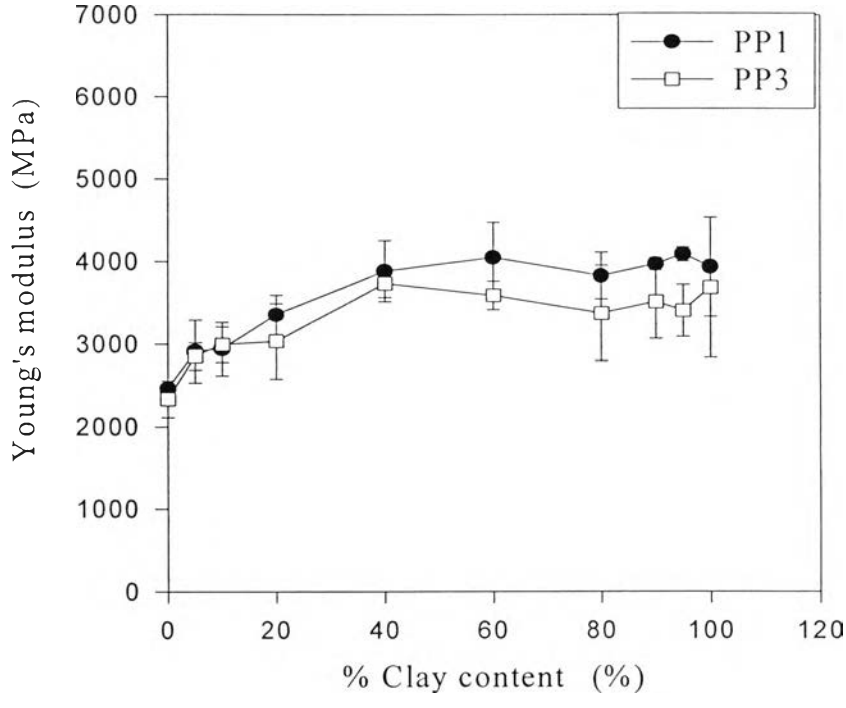

Figure 3.17 Effect of M_W on Young's modulus of 2/y/10 composites at 26°C.

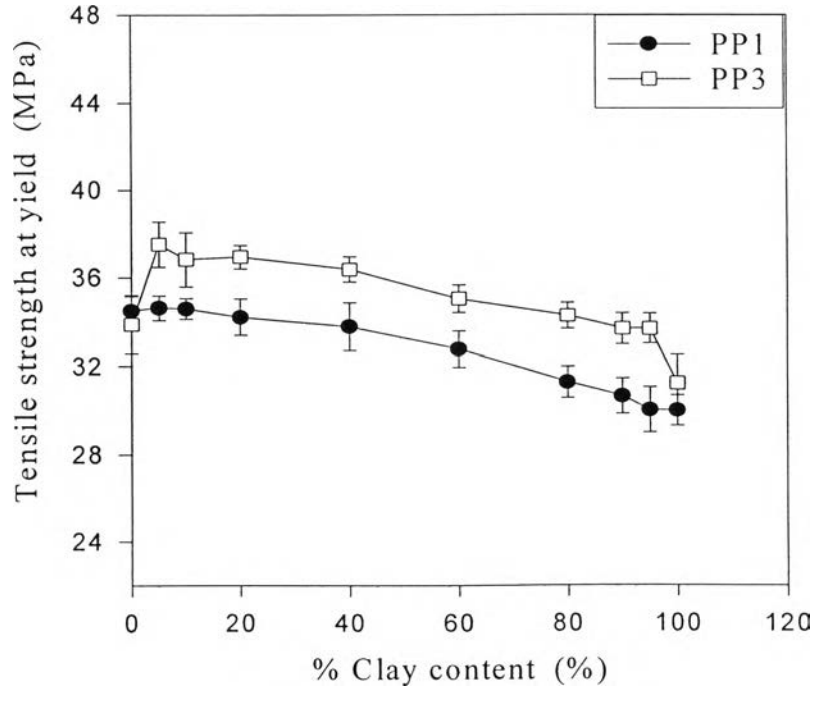

Figure 3.18 Effect of M_W on tensile strength at yield of 2/y/10 composites at 26°C.

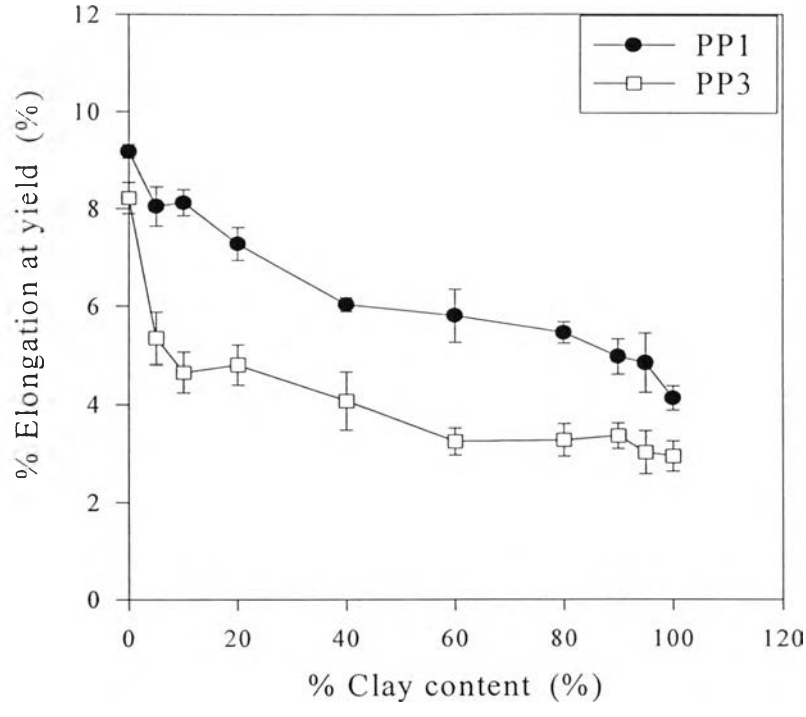

Figure 3.19 Effect of M_W on % elongation at yield of 2/y/10 composites at 26°C.

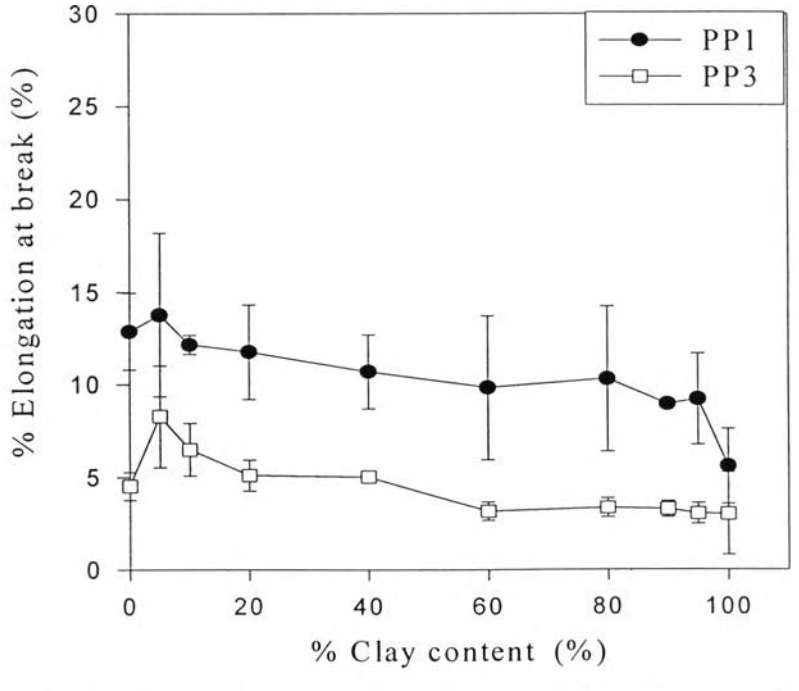

Figure 3.20 Effect of M_W on percent elongation at break of 2/y/10 composites at 26°C.

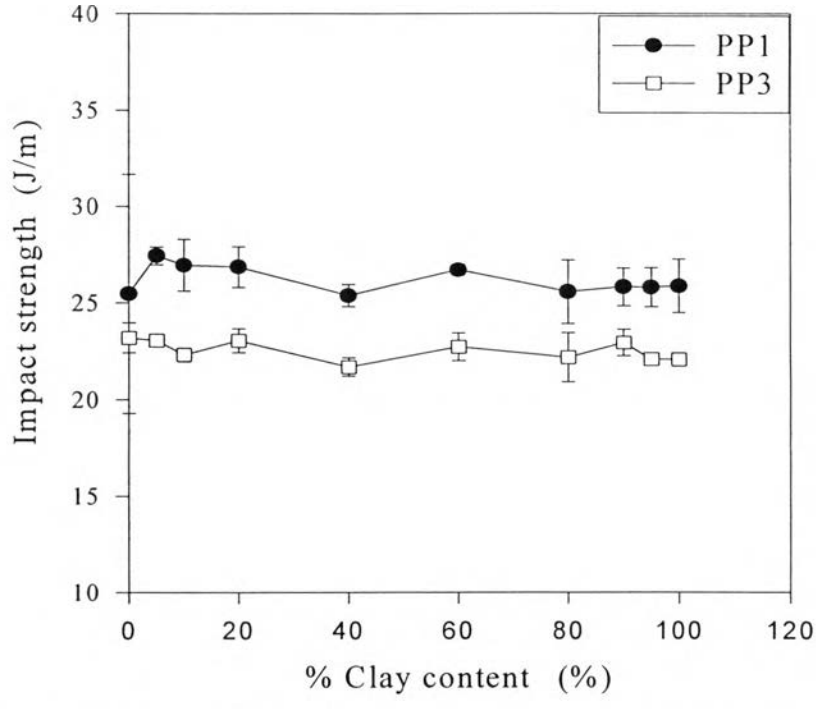

Figure 3.21 Effect of M_W on impact strength of 2/y/10 composites at 26°C.

The tensile and impact properties of PP1 and PP3 composites at fixed 10 wt % filler were plotted in Figures 3.17-3.21. The results of Young's modulus, tensile strength at yield, percent elongation at yield, percent elongation at break and impact strength show similar behaviors. PP1 composite properties have higher values in the Young's modulus, tensile strength and impact strength than those of PP3 composites. This is because the higher M_W polymer has a higher degree of entanglement. This results in higher stiffness, and longer tie molecules. It is easier for stress to transfer and the higher M_W polymer can absorb more energy before cracking.

3.3.2 Slow Crack Growth Properties

The crack growth behavier of pure PP1, pure PP3, PP1/2/20/10, PP3/2/20/10, PP1/2/60/10 and PP3/2/60/10 composites were investigated. The crack opening displacement (COD) and the crack length (CL) were measured as a function of time. They were measured by the Zoom stereomicroscope with

magnification 80x at the room temperature of 24°C. The crack opening displacement corresponds to the value of seperation distance at the initial notch tip. The crack length corresponds to the length of the stress whitening beyond the notch tip. For each measurement, the sample was taken off the slow crack growth apparatus for measuring the COD and CL. The duration of measurement when the sample was under no loading was a fraction of 0.69% of the total experimental time. The unloading time was negligible in our experiment.

3.3.2.1 Effect of M_W on the Slow Crack Growth Measurement.

When stress is applied to the structures, it can be expected that crystalline domains come apart as the tie molecules disengage from the crystals. The disengagement process is not known but it may involve the pulling of the tie molecules which hold them together. Based on this model, it is expected that the time to failure would be influenced mostly by the concentration of tie molecules since the force exerted by a tie molecule on the crystal is inversely proportional to the concentration of the molecules.

More recent work by Qian et al. [1993] on the effect of a solvent on the slow crack growth in PE suggested that entanglements in the amorphous region could also contribute to the resistance to the process of disentanglement. It was suggested that, when two molecules that emanated from adjoining crystals became strongly entangled, a tie molecule was formed.

Our result shows that time to propagate the crack increases with increasing M_W as shown in Figures 3.23-3.26. This is because of the increase in number of tie molecules with increasing M_W. Our result is consistent with the result of Huang and Brown [1988]. Their results showed that a large increase in the resistance to SCG occurred when the high side of M_W distribution was extended.

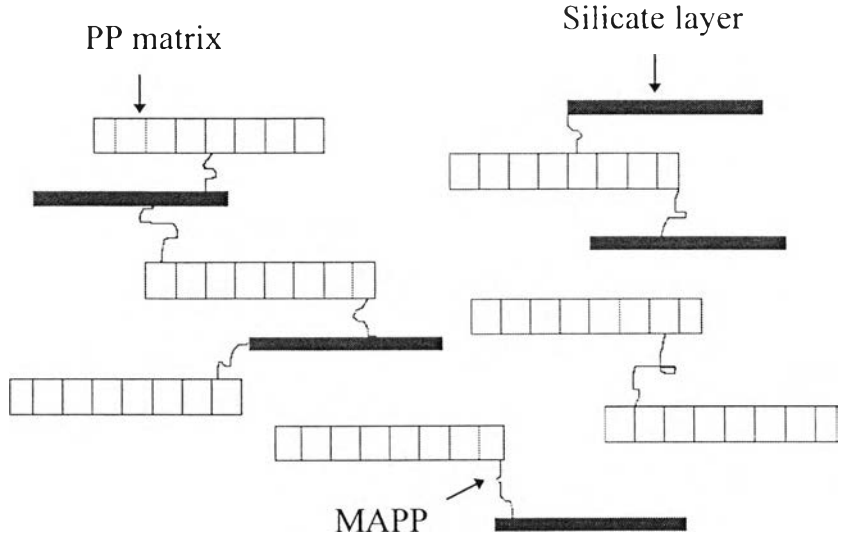

Figure 3.22 Model shows tie molecule in the nanocomposite.

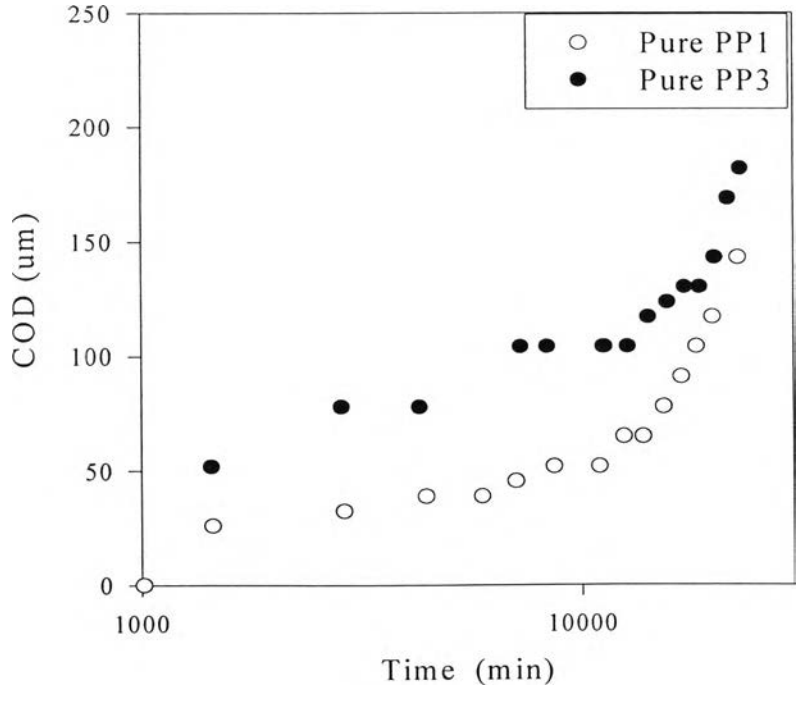

Figure 3.23 Crack opening displacement of pure PP1 and pure PP3.

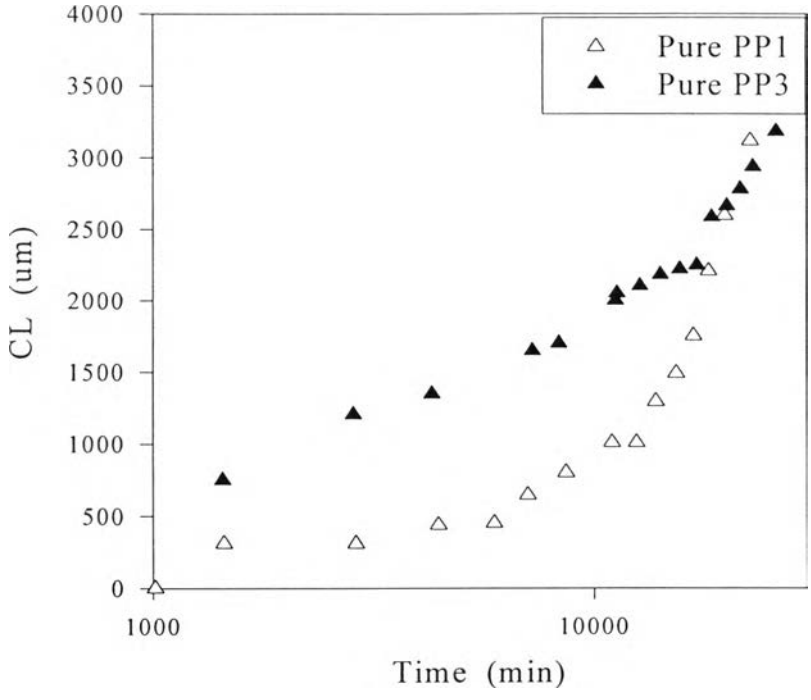

Figure 3.24 Crack length of pure PP1 and pure PP3.

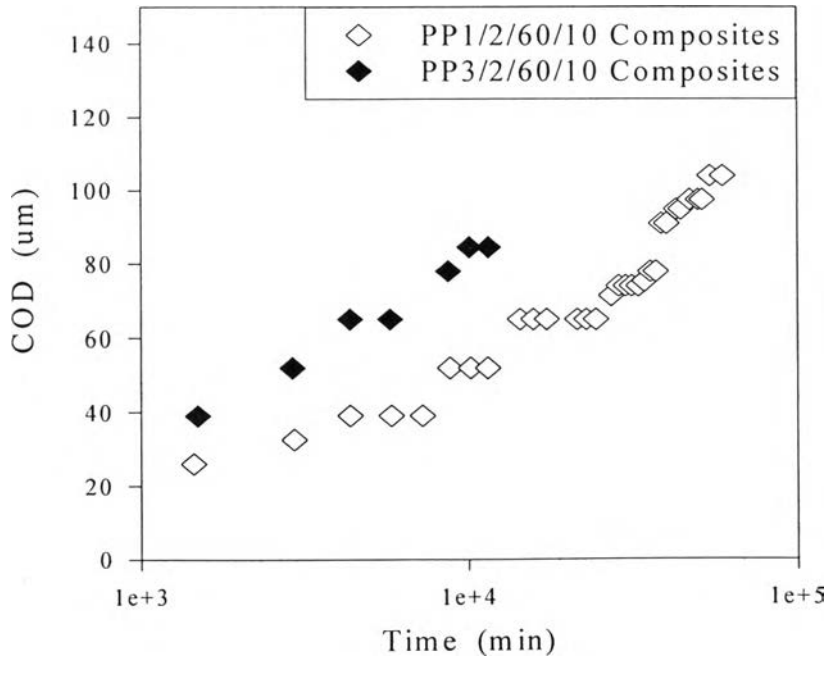

Figure 3.25 Crack opening displacement of PP1/2/60/10 composites and PP3/2/60/10 composites.

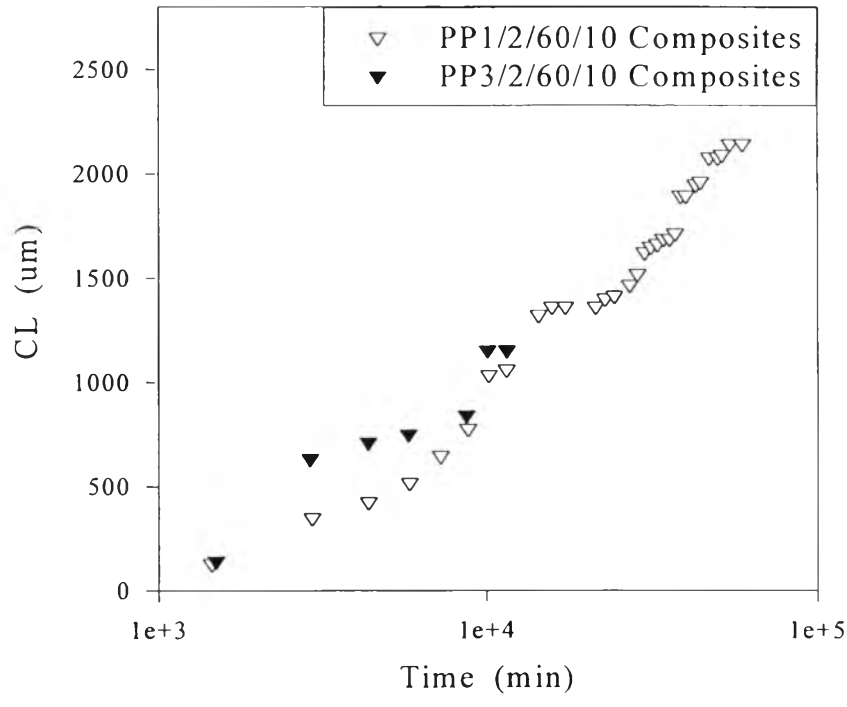

Figure 3.26 Crack length of PP1/2/60/10 composites and PP3/2/60/10 composites.

3.3.2.2 Effect of Clay Content on Slow Crack Growth Behavior.

The crack opening displacement and the crack length of pure PP3, PP3/2/20/10 composites and PP3/2/60/10 composites are shown in Figures 3.27 and 3.28. The results show that time to propagate the crack of pure PP3 is less than that of PP3/2/60/10 composites and PP3/2/20/10 composites respectively. Between the pure PP3 and PP3 composites, time to propagate the crack of PP3 composites is higher than pure PP3 because of the dispersed clay is of small particle size and possibly the good level of filler dispersion. This results in extra physical linking between crystalline structures. The tie molecules behave as a linkage device. Between the PP3/2/20/10 composites and the PP3/2/60/10 composites, the PP3/2/20/10 composites have a better resistance to crack propagation. This is because a higher content in MAPP results in higher concentration of tie molecules and finer degree of filler delamination. The results of crack opening displacement and the crack length of pure PP1,

PP1/2/20/10 composites and PP1/2/60/10 composites that are shown in Figures 3.29-3.30 show the same trend with pure PP3, PP3/2/20/10 and PP3/2/60/10 composites.

From the work of Lu et al. [1993], their microscopic view point suggested that the following sequence of events occurred in each composite:

(1) A craze was formed when the specimen was initially stressed.

(2) As the craze growed, the COD increased at a rate given by the initial slope of the COD versus time.

(3) At a critical value of the COD, δ_c, fracture initiated as indicated by the fracture of the fibrils at the base of the craze.

(4) For COD beyond δ_c, the crack growed with a craze as a precursor and the COD versus time curve accelerated until the specimen failed.

The phenomenon that determines the resistance to slow crack growth is the rate of extension of the fibrils which causes fracture to initiate at the base of the craze.

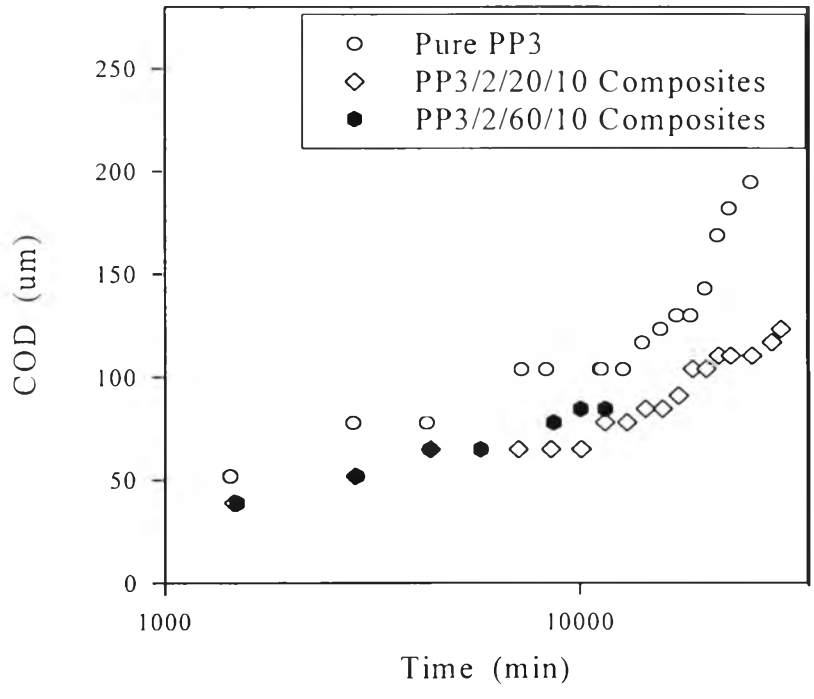

Figure 3.27 Crack opening displacement of pure PP3, PP3/2/20/10 composites and PP3/2/60/10 composites.

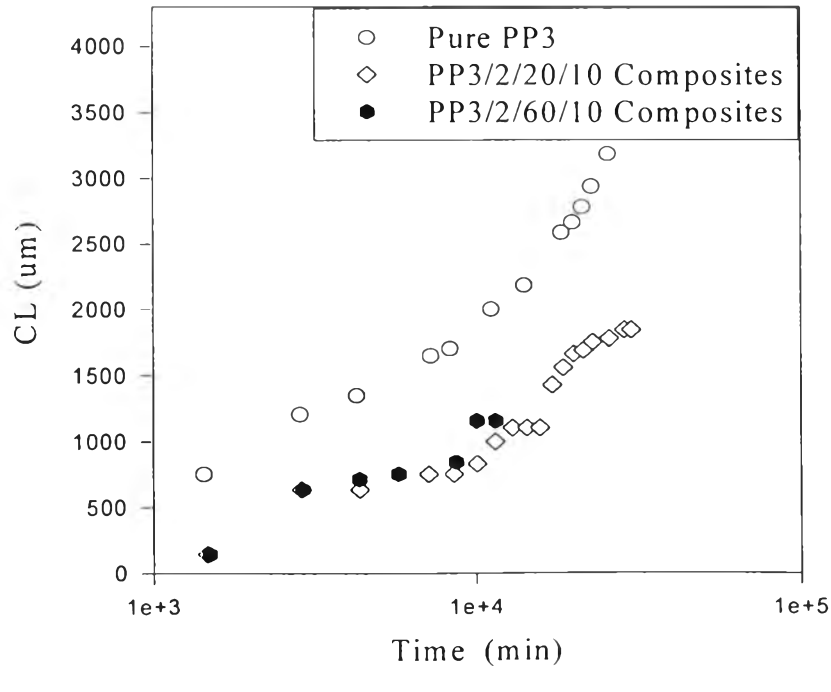

Figure 3.28 Crack length of pure PP3, PP3/2/20/10 composites and PP3/2/60/10 composites.

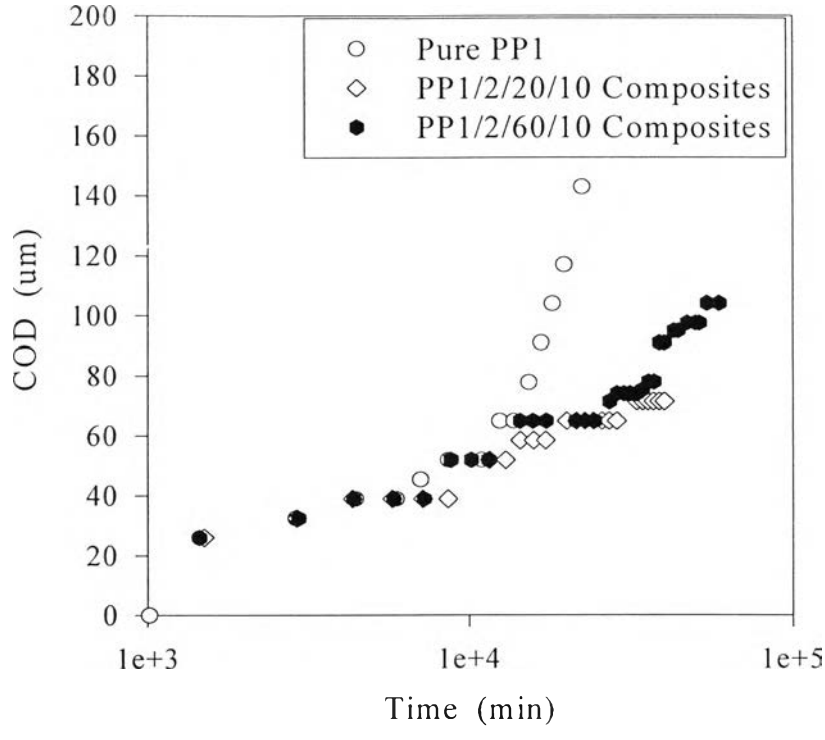

Figure 3.29 Crack opening displacement of pure PP1, PP1/2/20/10 composites and PP1/2/60/10 composites.

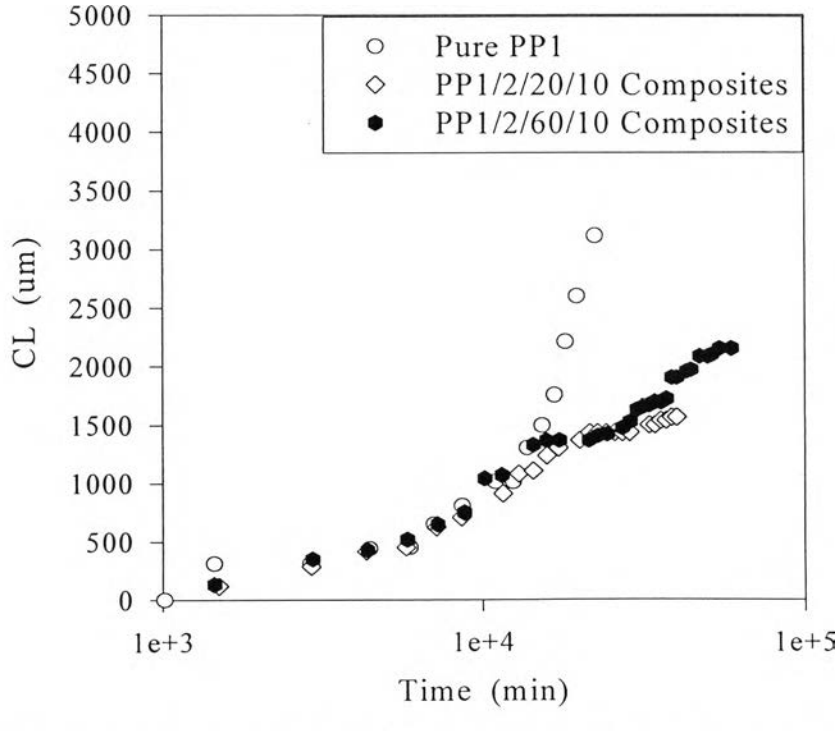

Figure 3.30 Crack length of pure PP1, PP1/2/20/10 composites and PP1/2/60/10 composites.